

Mathematical Modelling of Multirotor UAV

DENIS KOTARSKI, Mechanical Engineering, Karlovac University of Applied Sciences
Trg J.J. Strossmayera 9, CROATIA, denis.kotarski@vuka.hr

PETAR PILJEK, Faculty of Mechanical Engineering and Naval Architecture, University of Zagreb
Ivana Lucica 5, CROATIA, petar.piljek@fsb.hr

MATIJA KRZNAR, Peti Brod, Zlatarska 14, CROATIA, matija.krznar@petibrod.hr

Abstract: - Multirotor Unmanned Aerial Vehicles (UAV) are used in many applications such as surveillance, inspection operations, and disaster site observations. Mathematical model of a multirotor UAV is indispensable in movement simulation and later control design. Mathematical model is, at the same time, the first step in comprehending the mathematical principles and physical laws which are applied to the multirotor system. In this paper we derived movement matrix for multirotor UAV and analyse multirotor configuration to force and torque distribution in space. Because of different requirements for payload, agility, power consumption, manipulability, it is necessary to know which multirotor configuration is optimal for particular demand. Analysis results of multirotor configuration are graphically shown by force and torque ellipsoids. By changing the tilt angle, multirotor UAV is able to achieve full controllability over its 6 DOF body pose in space, respectively, it can decouple position from orientation.

Key-Words: - UAV, multirotor, 6 DOF, rigid body, Newton-Euler method, movement matrix, tilt angle

1 Introduction

Multirotor type of Unmanned Aerial Vehicles (UAV) are expected to have wide range of applications because they have capability of collecting the necessary information from the sky. Because of unique ability to carry out vertical take-off and landing (VTOL), stationary and low speed flight, these platforms are studied and designed, considering they are more and more applicable. Challenges for this type of UAV and opportunities to research are described [1].

UAVs can support disaster site observations or search and rescue missions. There are several solutions required for this scenarios. Some studies propose new design [2, 3] and new model [4]. For better design and model, also for control design, it is mandatory to discern physical parameters of proposed concept. Some papers show experimental identification of

physical parameters [5,6]. For manipulation with objects there are several groups that investigate novel concepts of actuation and multirotor configuration. They propose new prototypes [7,8]. During the inspection operations, aircrafts are very often struggling with wind gusts or other environmental disturbances. There have been some studies for using nonlinear control algorithms for trajectory tracking with disturbance rejection. [9,10].

Multirotor as an aircraft has six degrees of freedom – 6 DOF. Only moving parts on multirotor are propulsor propellers which are fixed in a propulsors axis. Multirotor frame is assumed to be symmetric and rigid. Direct influence on the multirotor movement is induced by variation of each motor's RPM. To achieve stable flight, it is necessary to combine several high accuracy sensors with fast and robust control algorithm.

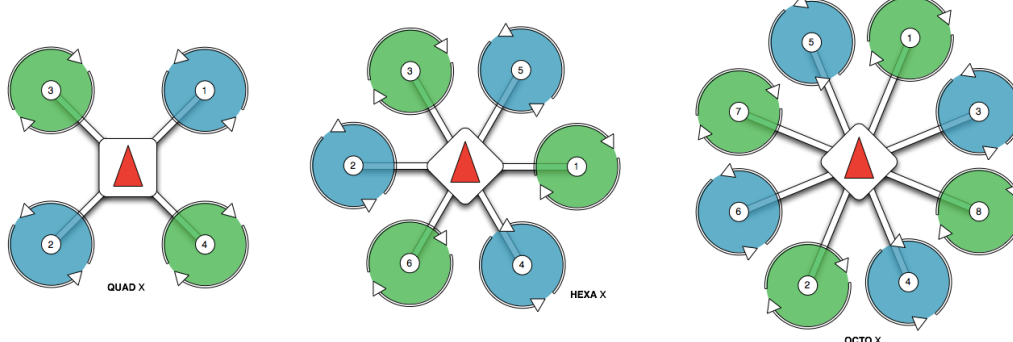


Fig. 1 Typical flat multirotor configurations (PixHawkTM motor layout)

2 Multirotor Mathematical Model

Mathematical model describes multirotor movement and behaviour with the respect to the input values of the model and external influences on multirotor. Mathematical model can be considered as a function that is mapping inputs on outputs. By using mathematical model, it is possible to predict position and attitude of multirotor by knowing the angular velocities of propellers, i.e. it enables computer simulation of multirotor behaviour in different conditions.

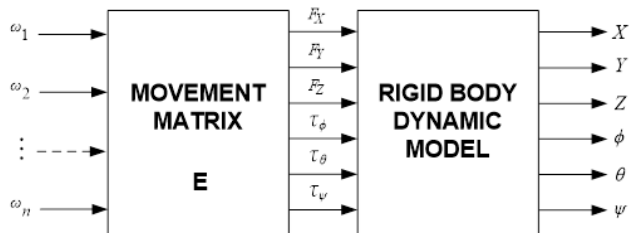


Fig. 2 Inputs and outputs of multirotor mathematical model

2.1 Rigid Body Kinematics

It is necessary to define two coordinate systems:

- Earth fixed frame (E-frame, \mathcal{F}^E)
- Body fixed frame (B-frame, \mathcal{F}^B)

Some multirotor physical properties are measured in \mathcal{F}^E , while some properties are measured in \mathcal{F}^B .

\mathcal{F}^E is the inertial right-handed coordinate system where positive direction of Z_E axis is in the direction normal to the earth ground level. Multirotor position $\xi = [X \ Y \ Z]^T$ and attitude $\eta = [\phi \ \theta \ \psi]^T$ are defined in \mathcal{F}^E . Roll-pitch-yaw convention order is applied.

\mathcal{F}^B is fixed on multirotor body. Positive direction of the X_B is pointing with red arrow (Fig. 2). \mathcal{F}^B is also right-handed coordinate system. Assumption is that the origin of \mathcal{F}^B coincides with the center of gravity (COG) of the multirotor. Linear velocities \mathbf{v}^B , angular velocities $\boldsymbol{\omega}^B$, forces \mathbf{f}^B and torques $\boldsymbol{\tau}^B$ are defined in \mathcal{F}^B .

Motion equations are more suitable to formulate with the respect to the \mathcal{F}^B for several reasons: system inertia matrix is time-invariant, equations simplification because of multirotor frame symmetry, sensors measurements are easily converted to \mathcal{F}^B and control variables equations simplification.

Kinematics of a rigid body with 6 DOF is given with:

$$\dot{\boldsymbol{\epsilon}} = \mathbf{J}\mathbf{v}, \quad (1)$$

where $\dot{\boldsymbol{\epsilon}} = [\dot{\xi} \ \dot{\eta}]^T$ is generalized velocity vector in \mathcal{F}^E , $\mathbf{v} = [\mathbf{v}^B \ \boldsymbol{\omega}^B]^T$ is generalized velocity vector in \mathcal{F}^B , and \mathbf{J} is generalized rotation and transformation matrix.

$$\mathbf{J} = \begin{bmatrix} \mathbf{R} & \mathbf{0}_{3 \times 3} \\ \mathbf{0}_{3 \times 3} & \mathbf{T} \end{bmatrix} \quad (2)$$

\mathbf{R} is the rotation matrix which maps linear velocity vector from one coordinate system to another

$$\mathbf{R} = \begin{bmatrix} C\psi C\theta & C\psi S\theta S\phi - S\psi C\phi & C\psi S\theta C\phi + S\psi S\phi \\ S\psi C\theta & S\psi S\theta S\phi + C\psi C\phi & S\psi S\theta C\phi - C\psi S\phi \\ -S\theta & C\theta S\phi & C\theta C\phi \end{bmatrix} \quad (3)$$

where $C_i = \cos(i)$, $S_j = \sin(j)$.

Because of the need to transform measured values from one coordinate system to another, the rotation matrix is introduced. Matrix \mathbf{T} is the transformation matrix that transfers angular velocities from \mathcal{F}^B to \mathcal{F}^E . Since hybrid coordinate system is used for deriving the dynamic model, the matrix \mathbf{T} is not used. Instead, velocity vector in hybrid coordinate frame (\mathcal{F}^H) is defined as $\zeta = [\xi \ \boldsymbol{\omega}^B]^T$.

2.2 Rigid Body Dynamics

Multirotor dynamics is described by differential equations that were derived by using the Newton-Euler method. Dynamics of a rigid 6 DOF body takes into consideration the mass m and the inertia of the body \mathbf{I} . By applying the assumption that the multirotor frame has symmetrical structure, i.e. the principal inertia axes coincides with the \mathcal{F}^B coordinate axes, inertia matrix becomes the diagonal matrix.

$$\mathbf{M}_B \ddot{\mathbf{v}} + \mathbf{C}_B(\mathbf{v})\dot{\mathbf{v}} = \boldsymbol{\lambda}, \quad (4)$$

where $\ddot{\mathbf{v}}$ is the generalized acceleration vector, \mathbf{M}_B is the system inertia matrix, $\mathbf{C}_B(\mathbf{v})$ is the Coriolis-centripetal matrix, all with the respect to the \mathcal{F}^B . Generalized force vector $\boldsymbol{\lambda} = [\mathbf{f}^B \ \boldsymbol{\tau}^B]^T$ can be divided into three components; gravitational vector $\mathbf{g}_B(\boldsymbol{\epsilon})$, gyroscopic torque vector $\mathbf{o}_B(\mathbf{v})\boldsymbol{\omega}$ and movement vector $\mathbf{u}_B(\boldsymbol{\omega})$.

$$\boldsymbol{\lambda} = \mathbf{g}_B(\boldsymbol{\epsilon}) + \mathbf{o}_B(\mathbf{v})\boldsymbol{\omega} + \mathbf{E}_B\boldsymbol{\omega}^2, \quad (5)$$

Gravitational vector only affects the linear components of the model, while gyroscopic torque vector only affects angular components of the model. Movement vector $\mathbf{u}_B(\boldsymbol{\omega})$ is represented by the product of movement matrix \mathbf{E}_B and the vector of the squared angular velocities of the propellers $\boldsymbol{\omega}^2$.

Dynamics of a rigid body with 6 DOF is given with:

$$\dot{\mathbf{v}} = \mathbf{M}_B^{-1}[-\mathbf{C}_B(\mathbf{v})\mathbf{v} + \mathbf{g}_B(\xi) + \mathbf{o}_B(\mathbf{v})\omega + \mathbf{E}\omega^2] \quad (6)$$

what, basically, is a matrix formulation of Newton's second law of motion.

Generalized acceleration vector with respect to \mathcal{F}^H can be calculated as

$$\dot{\zeta} = \mathbf{M}_H^{-1}[-\mathbf{C}_H(\zeta)\zeta + \mathbf{g}_H + \mathbf{o}_H(\zeta)\omega + \mathbf{E}\omega^2] \quad (7)$$

2.3 Force/Torque Mapping

Based on multirotor configuration and propulsion geometric arrangement, a movement matrix can be derived. At first, it is necessary to provide kinematic analysis of the connection between force/torque actuation and propulsion configuration.

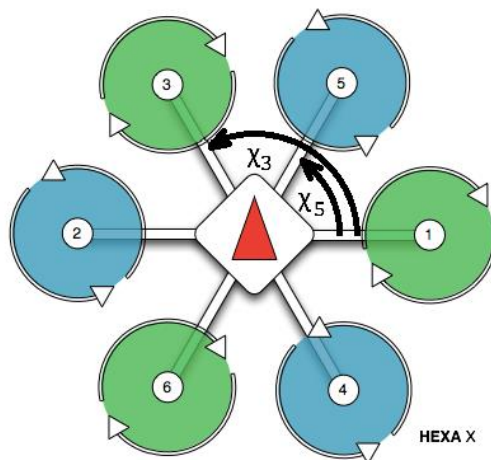


Fig. 3 Multirotor configuration – Hexa X

Multirotor configuration consists of arbitrary number of propulsions (PN). Each propulsion generates an aerodynamic force which consists of thrust force and drag moment.

Propulsion position ξ_{Pi} is defined as

$$\xi_{Pi} = \begin{bmatrix} \sin \chi_i \\ -\cos \chi_i \\ 0 \end{bmatrix} \cdot l \quad (8)$$

Where χ_i is the i-th propulsion position relative to the \mathcal{F}^B (Fig. 3), and l is the distance from rotor to COG.

Propulsion orientation $\boldsymbol{\eta}_{Pi}$ is defined as:

$$\boldsymbol{\eta}_{Pi} = \mathbf{CR} \cdot \begin{bmatrix} \sin \chi_i \cdot \sin \gamma \\ -\cos \chi_i \cdot \sin \gamma \\ \cos \gamma \end{bmatrix} \quad (9)$$

Where γ represents propulsion tilt angle. If $\gamma = 0$, then we have a common "flat" multirotor

configuration which means that we have underactuated system.

\mathbf{CR} is configuration rotation matrix and it describes a tilt angle signum with respect to XY plane in \mathcal{F}^B as shown in Fig. 4.

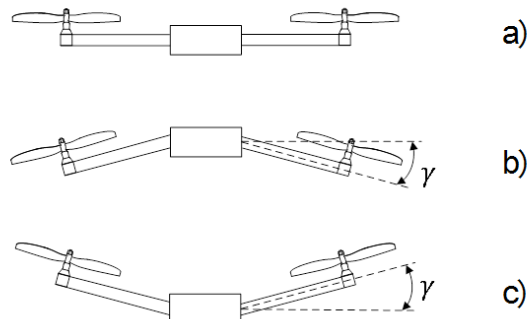


Fig. 4 Multirotor configuration rotation

Fig. 4a) shows a "flat" configuration. In b) case configuration rotation matrix is

$$\mathbf{CR} = \begin{bmatrix} 1 & 0 & 0 \\ 0 & 1 & 0 \\ 0 & 0 & 1 \end{bmatrix} \quad (10)$$

In c) case configuration rotation matrix is

$$\mathbf{CR} = \begin{bmatrix} -1 & 0 & 0 \\ 0 & -1 & 0 \\ 0 & 0 & 1 \end{bmatrix} \quad (11)$$

After kinematic analysis of multirotor configuration in \mathcal{F}^B is presented, analysis of propulsion system dynamics can be derived. Forces and torques that are generated by propulsion, directly effect on the multirotor position and orientation in space.

Each propulsion generates force vector which can be calculated by the following equation

$$\mathbf{f}_i = (\boldsymbol{\eta}_{Pi} \cdot b)\omega_i^2 \quad (12)$$

where ω_i is angular speed of the ith rotor, and b is the thrust coefficient [Ns^2].

Each propulsion also generates torque vector which can be calculated by the following equation

$$\boldsymbol{\tau}_i = (\boldsymbol{\xi}_{Pi} \times \boldsymbol{\eta}_{Pi} \cdot b + PR \cdot \boldsymbol{\eta}_{Pi} \cdot d)\omega_i^2 \quad (13)$$

where d is the drag coefficient [Nms^2], and PR is the signum of propulsion rotation.

$$PR = \begin{cases} 1 & \text{if } i = CW \\ -1 & \text{if } i = CCW \end{cases}$$

From the static thrust test, constants b and d can be obtained. They depend on the propeller radius, thrust and power factor, and air density.

The generalized force vector $\mathbf{f}^B = [F_X \ F_Y \ F_Z]^T$ is defined as

$$\mathbf{f}^B = \sum_{i=1}^{PN} \mathbf{f}_i \quad (14)$$

The same way torque vector $\boldsymbol{\tau}^B = [\tau_x \ \tau_y \ \tau_z]^T$ is defined as

$$\boldsymbol{\tau}^B = \sum_{i=1}^{PN} \boldsymbol{\tau}_i \quad (15)$$

From equations 14 and 15, a movement matrix can be derived. The tilt angle decides how much force we can put into $[\tau_x \ \tau_y \ F_Z]^T$ or into $[F_X \ F_Y \ \tau_z]^T$. Considering aerodynamic effects, it follows that forces and moments are proportional to the squared angular velocities of the propellers. Movement vector $\mathbf{u}_B(\omega) = [\mathbf{f}^B \ \boldsymbol{\tau}^B]^T$ is represented by the product of movement matrix \mathbf{E}_B and the vector of the squared angular velocities of the propellers $\boldsymbol{\omega}^2$. As shown in Fig. 2, movement vector is input in rigid body dynamic model.

$$\mathbf{u}_B(\omega) = \mathbf{E}_B \boldsymbol{\omega}^2 \quad (16)$$

For the control design and implementation on an aircraft prototype, it is necessary to calculate the angular velocity for each individual propulsion

$$\boldsymbol{\omega}^2 = \mathbf{E}_B^{-1} \mathbf{u}_B \quad (17)$$

3 Tilt angle analysis

We provide analysis for hexarotor X configuration as shown in Fig. 3 with configuration rotation matrix as shown in Fig. 3c. Tilt angles are presented in Table 1. The tilt angle indicates how much force we can put into $[\tau_x \ \tau_y \ F_Z]^T$ or into $[F_X \ F_Y \ \tau_z]^T$.

Table 1

Tilt angle γ [°]				
0	2	4	6	8
10	12	15	18	20

Clearly at $\gamma = 0^\circ$, there are no forces in XY plane in \mathcal{F}^B and torque around Z axis is relatively small, so there is no ability to control F_X and F_Y directly.

Tilt angle analysis is especially important for further study of agility, power consumption, component selection, effects of platform size, disturbance rejection, etc.

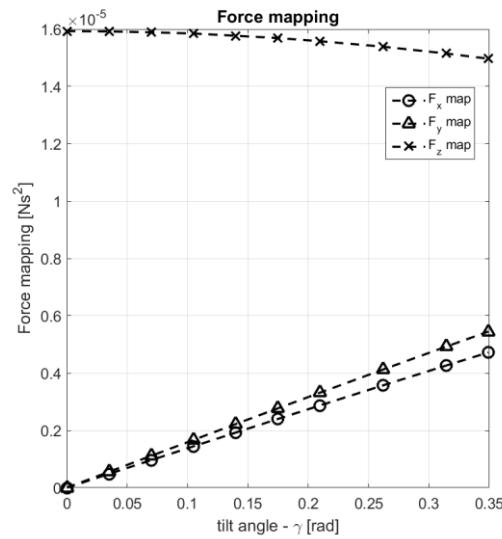


Fig. 5 Maximum available force map values at different tilt angles

It can be seen from Fig. 5 that the multirotor maximum available force map values depend on tilt angle. Force maps also depend on chosen motors and multirotor dimensions. As the tilt angle increases, the force along the Z axis falls and it is necessary to increase the angular velocities of propulsion in order to keep a hover. Opposite of Z axis, force along the X and Y axis grows.

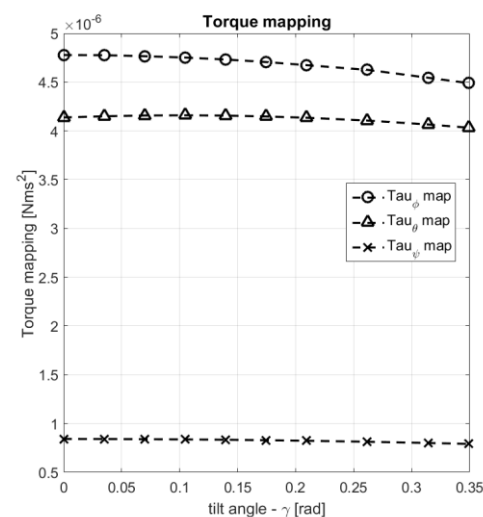


Fig. 6 Maximum available torque map values at different tilt angles

Fig. 6 shows the multirotor maximum available torque map values depending on tilt angle. As the tilt angle increases, torques slightly decreases.

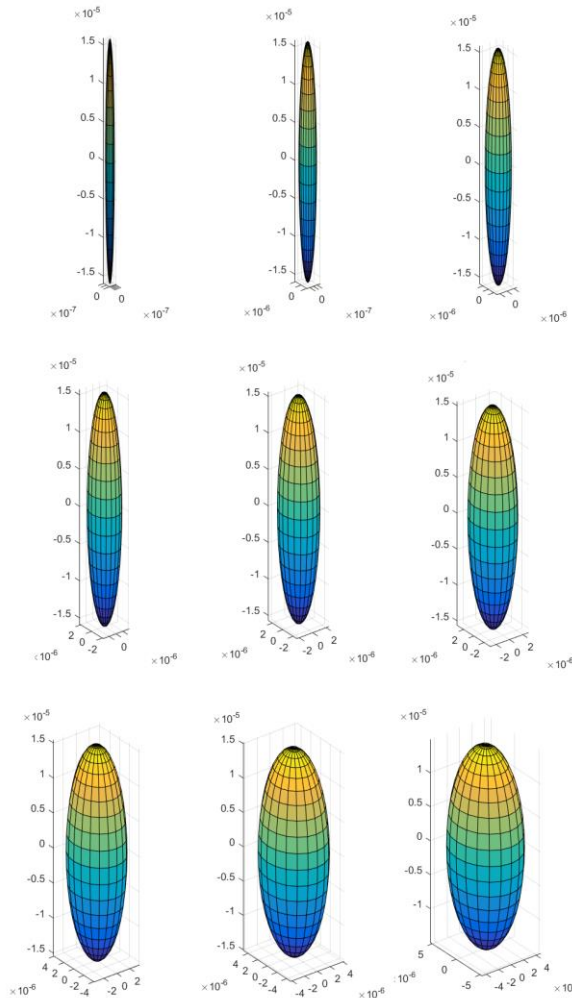


Fig. 6 Maximum available torque map values depending on tilt angle

Fig. 7 shows the force ellipsoids which depends on the tilt angle (Table 1). The first image represents the ellipsoid for tilt angle 2° and the last is for 20° . As it can be seen, with increasing tilt angle, we get a control over F_X and F_Y . Hence, we have a fully actuated system.

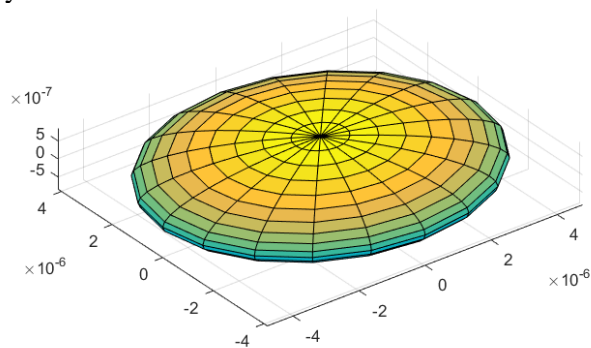


Fig. 7 Force ellipsoids for different tilt angles

4 Simulation results

The behaviour of the outputs of the mathematical model is dependent on the input values. Even though the mathematical model deals with angular velocities as one of the variables, the input values are chosen to be the RPM of the propellers ($n = \frac{30\omega}{\pi}$) because that is the more natural way of setting the propeller rotation. The outputs of the model are multirotor position and orientation. Based on the estimated physical parameters, which are needed for calculating the output values, input values can be given for which the multirotor will behave in the expected way.

Described movement matrix has been validated with the simulation results in related work [11].

Table 2 Mathematical model input parameters

t	RPM [rev/min]					
	M ₁	M ₂	M ₃	M ₄	M ₅	M ₆
0-5sec	3480	3480	3480	3480	3480	3480
5-10sec	3480	3480	3479	3481	3479	3481

The state of constant altitude is wanted to be achieved. After 5th second, forward movement is wanted. As shown in Fig. 9, for the first 5 seconds multirotor maintain constant altitude. After 5th second, multirotor is going forward with drop in height.

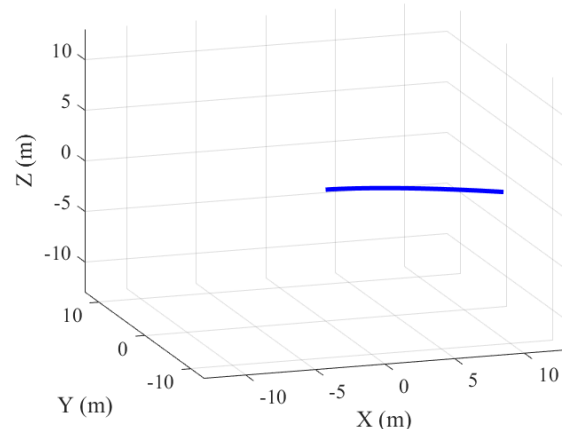


Fig. 9 Multirotor position during simulation

5 Conclusion

In this paper the complexity of the multirotor mathematical model derivation is shown. Dynamic model consists of rigid body dynamics model and movement matrix. The key contribution of this paper is derivation of the movement matrix \mathbf{E}_B for a class of multirotors and to analyse multirotor configuration

influence on movement matrix. This matrix is used for mapping the angular velocity to force/torque. As it can be seen, by changing tilt angle, full controllability of multirotor UAV can be achieved over its 6 DOF body pose in space. It means that roll angle can be decoupled from the Y-translation and the pitch angle from the X-translation.

By running several simulations with various tilt angle, force and torque ellipsoids can be obtained as shown in Fig. 7 and Fig. 8. These ellipsoids represent available force in space as a function of tilt angle. As it can be seen, the available force in XY plane increases as tilt angle increase.

Further work will include control design for various configuration with stability analysis and mathematical model improvements.

References:

- [1] V. Kumar, N. Michael, Opportunities and challenges with autonomous micro aerial vehicles, *The International Jurnal of Robotics Research*, 2012.
- [2] A. Kalantari, Design and Experimental Validation of HyTAQ, a Hybrid Terrestrial and Aerial Quadrotor, *IEEE International Conference on Robotics and Automation (ICRA)*, 2013.
- [3] S. Mizutani, Y. Okada, C. J. Salaan, T. Ishii, K. Ohno and S. Tadokoro, Proposal and Experimental Validation of a Design Strategy for a UAV with a Passive Rotating Spherical Shell, *IEEE/RSJ International Conference on Intelligent Robots and Systems (IROS)*, 2015.
- [4] A. Briod, P. Kornatowski, J.C. Zufferey, D. Floreano, A Collision-resilient Flying Robot, *Journal of Field Robotics*, 31(4), pp. 496–509, 2014.
- [5] A. Bondyra, S. Gardecki, P. Gasior and W. Giernacki, Performance of Coaxial Propulsion in Design of Multi-rotor UAVs, *Challenges in Automation*, Springer International Publishing Switzerland, 2016.
- [6] M. Yoon, Experimental Identification of Thrust Dynamics for a Multi-Rotor Helicopter, *International Journal of Engineering Research & Technology (IJERT)*, Vol.4, No.11, 2015
- [7] M. Ryll, H. H. Bülthoff, P. R. Giordano, A Novel Overactuated Quadrotor Unmanned Aerial Vehicle: Modeling, Control, and Experimental Validation, *IEEE Transactions on Control Systems Technology*, pp 1063-6536, 2014.
- [8] G. Jiang, R. Voyles, A Nonparallel Hexrotor UAV with Faster Response to Disturbances for Precision Position Keeping, *SSRR*, 2014.
- [9] J. Kasać, S. Stevanović, T. Žilić, J. Stepanić, Robust Output Tracking Control of a Quadrotor in the Presence of External Disturbances, *Transactions of FAMENA*, 37(4), pp. 29-42, 2013.
- [10] S. Rajappa, C. Masone, H. H. Bulthoff, P. Stegagno, Adaptive Super Twisting Controller for a Quadrotor UAV, *IEEE International Conference on Robotics and Automation (ICRA)*, 2016.
- [11] Z. Benić, P. Piljek, D. Kotarski, Mathematical modelling of unmanned aerial vehicles with four rotors, *Interdisciplinary Description of Complex Systems*, 14(1), pp. 88-100, 2016.